

Proceedings of the 11th Polish–Japanese Joint Seminar on Micro and Nano Analysis, Gniez, September 11–14, 2016

# *In Situ* Electron Beam Amorphization of $\text{Sb}_2\text{Te}_3$ within Single Walled Carbon Nanotubes

S.R. MARKS<sup>a</sup>, K. MORAWIEC<sup>b</sup>, P. DLUZEWSKI<sup>b</sup>, S. KRET<sup>b</sup> AND J. SLOAN<sup>a,\*</sup>

<sup>a</sup>Department of Physics and School of Engineering, University of Warwick, Coventry, CV4 7AL UK

<sup>b</sup>Institute of Physics, Polish Academy of Sciences, al. Lotnikow 32/46, PL-02668 Warsaw, Poland

In this study, we reveal the crystallography, crystallinity, and amorphization of low-dimensional crystals of the topological insulator and phase change material  $\text{Sb}_2\text{Te}_3$  within both discrete and bundled single walled carbon nanotubes with a diameter range spanning 1.3–1.7 nm by a combination of electron diffraction, aberration-corrected high resolution imaging, and variable dose electron beam irradiation. We further reveal that electron diffraction indicates that the crystallinity of the host single walled carbon nanotubes is largely unaffected by this process indicating that mass loss during the observed *in situ* glass transition had not occurred and that the template had maintained its structural integrity. Such a transition would not be possible with any other common nanoporous template for which the pores would be enlarged due to likely sintering.

DOI: [10.12693/APhysPolA.131.1324](https://doi.org/10.12693/APhysPolA.131.1324)

PACS/topics: 61.82.Rx, 62.23.Hj, 64.70.Nd, 64.70.P-, 61.80.Fe, 61.72.Dd, 61.48.De

## 1. Introduction

Driven by a growing demand for high-density data storage materials, local phase change behaviour in nanoscale “phase change materials” (PCMs) has been studied by scanning probe microscopies based on conductance modification [1–3], ferroelectric polarization [4] and topographic transformation [5–7]. Recently, a variety of PCMs, including GeTe [8], SnSe [9] and PbTe [10] have been incorporated into single walled carbon nanotubes (SWNTs) to produce, in effect, “nano-confined” PCMs or nC-PCMs. These confining systems have several significant advantages over many other comparable templated composite systems: (i) the internal van der Waals surface of SWNTs constrains the size of the nC-PCMs to atomically smooth nanopores with confining surfaces as small as *ca.* 1 nm<sup>2</sup> in cross-section [8]; (ii) by comparison with porous templates fabricated from, for example, anodic alumina [11] or nanoporous or mesoporous silica [12], SWNTs in particular are thermally robust to 1400 K and, crucially, do not sinter or otherwise structurally rearrange over this temperature range [13]; and (iii) are only selectively sensitive to electron beam irradiation under moderate to medium electron beam dose conditions below the threshold for knock on electron beam damage, i.e. 86 keV [14]. When SWNTs are filled with PCMs, such as GeTe [8] or SnSe [9], it is therefore possible to rearrange the contained materials selectively either by *in situ* electron beam heating or by *ex situ* heating with minimal damage to the templating nanotubes.

If the templating nanotubes are undamaged during *in situ* modification of phase change materials and, providing there is no mass loss during a crystalline-to-glass

phase transition, then in principle the phase change can be made reversible. Following related investigations [8, 9] we seek here to investigate the *in situ* phase transformation characteristics of  $\text{Sb}_2\text{Te}_3$ , a material which exhibits high crystallinity inside SWNTs under ambient conditions but which undergoes a facile crystalline to glass phase transition at a moderate temperature or under moderate electron beam irradiation. In the bulk, unalloyed  $\text{Sb}_2\text{Te}_3$  melts at 580 °C but also undergoes significant melting and recrystallization in the presence of an electron beam [15]. The electrical charge carrier mobility and thermoelectric characteristics of thin films and bulk  $\text{Sb}_2\text{Te}_3$  are profoundly influenced by both thermal processing and by local crystallinity [16, 17]. In the present study, we describe the crystallinity and amorphization of  $\text{Sb}_2\text{Te}_3$  nanowires encapsulated within assemblies or bundles of SWNTs. We also show how this can be done without significant damage to the SWNTs at low accelerating voltage (i.e. < 86 kV) and at electron beam dosages ranging from 0.8 to 1.5 pA cm<sup>-2</sup>.

## 2. Experimental procedure and results

For this work we employed ultra-high purity SuperPureTubes™ SWNTs supplied by NanoIntegris with a diameter range 1.2–1.7 nm and < 1–3.5% catalyst impurity and less than 1–5% carbon impurity, supplied in unseparated “bucky paper” form. Prior to filling by the capillary method [18], these SWNTs were pretreated, due to their local adhesion, by ultrasonication in chloroform using a Cole-Parmer 750W Homogenizer at 20% power with 2 s on/off pulsing for 10 min. The dispersed SWNTs were gently dried on filter paper and then heated to 390 °C in an alumina boat in air in a Carbolite tube furnace to prepare them for the filling step [18]. Liquid phase filling was achieved by intimately grinding an equal volume of  $\text{Sb}_2\text{Te}_3$  (Sigma-Aldrich  $\approx$  325 mesh, 99.96%) with 20 mg of pre-treated SWNTs in an agate mortar and pestle, and

\*corresponding author; e-mail: [j.sloan@warwick.ac.uk](mailto:j.sloan@warwick.ac.uk)

then by heating the composite in a sealed silica quartz ampoule at 630 °C in the Carbolite furnace. Selected area electron diffraction (ED) patterns were obtained either on photographic plates in a JEOL 2000EX transmission electron microscope (TEM) and also a at a low beam dose ( $< 0.8 \text{ pA cm}^{-2}$ ) from bundles of both unfilled and filled SWNTs ranging from *ca.* 100–150 nm thick in projection (Fig. 1).

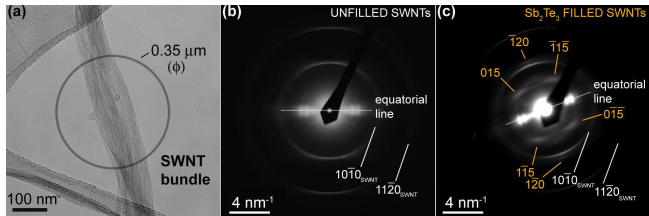


Fig. 1. (a) Low-magnification TEM image of a 120 nm diameter unfilled SWNT with the diameter ( $\varphi$ ) of the ED aperture indicated. (b) ED pattern from an unfilled SWNT bundle. Three prominent features are evident — the 1010 and 1120 rings and an equatorial line general to SWNT bundle diffraction [19]. (c) ED pattern from SWNTs bundle filled with crystalline  $\text{Sb}_2\text{Te}_3$ . Superimposed on the indicated diffraction features of the SWNT bundle are additional reflections corresponding to the  $\text{Sb}_2\text{Te}_3$  filling.

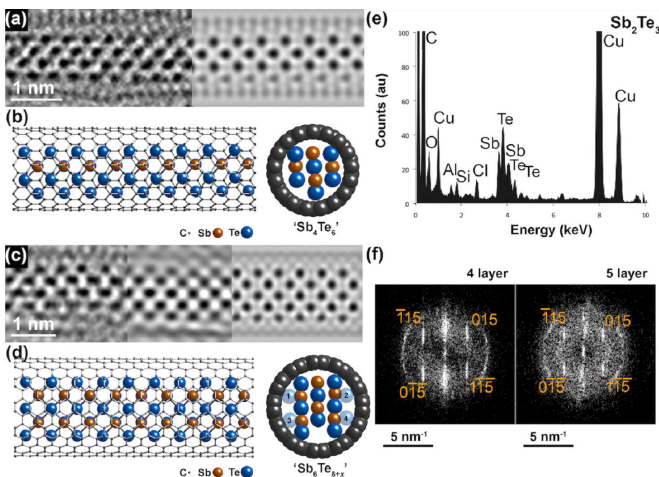


Fig. 2. (a) AC-TEM image (left), multislice image simulation (right) of a 4-atomic layer thick of a stoichiometric  $\text{Sb}_2\text{Te}_3$  fragment in a 1.35 nm diameter SWNT. (b) Structure models with stoichiometry tailored to  $\text{Sb}_4\text{Te}_6$ ; (c) AC-TEM image (left), Wien filtered image (middle) and multislice simulation (right) of a 5-atomic layer thick model of  $\text{Sb}_2\text{Te}_3$  in a  $\approx 1.62$  nm thick SWNT. (d) Structure models with the local stoichiometry tailored to  $\text{Sb}_6\text{Te}_{8+x}$ . This may be restored to  $\text{Sb}_2\text{Te}_3$  if there are  $x = 3$  ad-atoms per  $\text{Sb}_6\text{Te}_8$  fragment at positions 1–4. (e) EDX spectrum of SWNT bundle filled with  $\text{Sb}_2\text{Te}_3$  (Cu, Si, Al and Cl peaks are all background). (f) FFTs obtained from AC-TEM images in (a) and (b) revealing spatial frequencies corresponding to  $\{015\}$  lattice planes (and equivalent planes) in both fragments.

Additional TEM images and ED patterns of  $\text{Sb}_2\text{Te}_3$  encapsulated within SWNTs and also electron beam irradiation studies were performed in a dual (i.e. imaging and probe corrected) aberration corrected JEOL JEM-ARM200F instrument equipped with a Faraday cup, operating at 80 kV with the coefficient of spherical aberration tuned to  $\approx 1 \mu\text{m}$ . The TEM images were recorded on a Gatan SC-1,000 Orius CCD camera. Figure 2a–d shows high-resolution lattice images from individual filled SWNTs also obtained on this instrument (Fig. 2a–d). Local glass transformation of  $\text{Sb}_2\text{Te}_3$  in SWNT bundles was achieved in the JEM-ARM200F at 80 kV by gradually increasing the 80 kV electron beam dose from  $0.8 \text{ pA cm}^{-2}$  to  $1.5 \text{ pA cm}^{-2}$ . Increasing the electron beam dose much beyond  $1.5 \text{ pA cm}^{-2}$  tended to be deleterious to the SWNT bundle microstructure due to expected radiolysis [20]. X-ray microanalyses were performed on multiple  $\text{Sb}_2\text{Te}_3$  filled SWNT bundles to verify the elemental composition of the former (Fig. 2e) both pre- and post beam irradiation. In general, no overall change in composition was observed.

The diameter range of the supplied Nanointegris SWNTs spans 1.2–1.7 nm and we both expected and observed some variability in the microstructure of the  $\text{Sb}_2\text{Te}_3$  encapsulated nanocrystals as a function of the confining internal van der Waals surface of the SWNTs, expressed in terms of the inner diameter [21]. Any such variability in crystallography must be taken into account when considering the global scattering properties of this or indeed any other crystalline filling with nanotubes (i.e. Fig. 1c) but for  $\text{Sb}_2\text{Te}_3$  we find that this material undergoes a systematic “layer by layer” crystal growth inside SWNTs determined by the confining diameter (Fig. 2a–d). In *ca.* 1.3–1.4 nm diameter SWNTs (Figs. 2a and b), four layer thick fragments of  $\text{Sb}_2\text{Te}_3$  were observed and in  $\approx 1.5$ –1.65 nm diameter SWNTs (Figs. 2c and d), five layer thick fragments were observed.

Fast Fourier transforms (FFTs) obtained from 4 and 5-layer fragments of  $\text{Sb}_2\text{Te}_3$  in SWNTs (Fig. 2f) reveal prominent 0.315 nm (i.e.  $d_{\{015\}}$ ) spatial frequencies that are clearly reproduced in ED patterns obtained from bundles of nanotubes filled with this material (i.e. Fig. 1c). The crystalline origin of the 0.315 nm  $d_{\{015\}}$  spatial frequencies relative to the bulk  $\text{Sb}_2\text{Te}_3$  crystal structure is outlined in Fig. 3a–c for the 4-layer  $\text{Sb}_2\text{Te}_3$  fragment which is derived from a slice of the bulk  $\text{Sb}_2\text{Te}_3$  structure and is viewed in an oblique projection (i.e.  $[2.7, 1.4, 0.26]$ ) (Fig. 3b) relative to the bulk unit cell of  $\text{Sb}_2\text{Te}_3$ . An ED simulation corresponding to this projection (Fig. 3c) reproduces the  $d_{\{015\}}$  and complementary  $d_{\{1\bar{1}5\}}$  reflections also (cf. Figs. 1c and 2f). Also visible are reflections corresponding to longitudinal  $\{120\}$  lattice planes (indicated in Fig. 3b) which are clearly visible in ED patterns obtained from SWNT bundles (Fig. 1c).

The crystallinity of  $\text{Sb}_2\text{Te}_3$  in both bundled SWNTs (Fig. 1c) and also discrete SWNTs (Fig. 2a–d) and the associated crystallography, which are observed under moderate electron beam dose conditions, form a potential

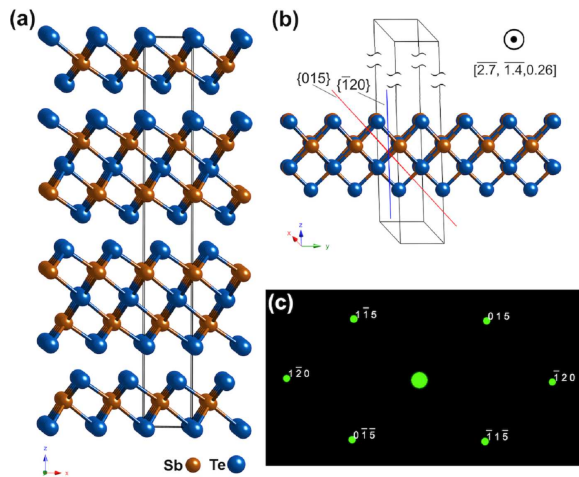


Fig. 3. (a)  $R\bar{3}mH$  unit cell of  $Sb_2Te_3$  [17] viewed along  $[010]$ ; (b) derivation of the 4-layer  $Sb_2Te_3$  from (a) but which is viewed in an oblique  $[2.7, 1.4, 0.26]$  projection relative to (a) which contains the  $\{015\}$  and  $\{\bar{1}20\}$  lattice planes; (c) ED simulation corresponding to the  $[2.7, 1.4, 0.26]$  projection — this reveals the most prominent diffraction features produced from bundles of 1.2–1.7 nm diameter SWNTs filled with crystalline  $Sb_2Te_3$  prior to the *in situ* glass transformation (i.e. Fig. 4a and b).

starting point for identifying crystalline to glass phase transitions in larger scale SWNT sample by analogy with bulk behaviour [15]. For  $Sb_2Te_3$ , two methods of producing crystalline to glass transitions are possible: (i) heating this material to above the melting temperature  $580^\circ\text{C}$  followed by rapid quenching, for example, in ice water [22], or (ii) electron beam irradiation above some minimum electron flux threshold [15]. Bundles of SWNTs filled initially with crystalline  $Sb_2Te_3$  were therefore subjected to low to moderate electron beam doses ranging from  $0.8\text{ pA cm}^{-2}$  to  $1.5\text{ pA cm}^{-2}$  in the time-resolved images reproduced in Fig. 4a and b. At the lower  $0.8\text{ pA cm}^{-2}$  electron beam dose, adjusted by varying the strength of the condenser lens in the AC-TEM, the crystallinity of  $Sb_2Te_3$  is retained as in the earlier example (i.e. cf. Figs. 1c and 4a). As the electron beam dose was gradually adjusted from  $0.8\text{ pA cm}^{-2}$  (i.e. Fig. 4a) to  $1.5\text{ pA cm}^{-2}$  (i.e. Fig. 4b) complete phase transformation was affected in less than 5 min. Significantly, the underlying diffraction features of the SWNTs are largely unaffected by this beam irradiation while the encapsulated  $Sb_2Te_3$  is completely transformed to the glassy phase.

### 3. Discussion and conclusions

In this brief study, we report three significant and interrelated observations for crystalline  $Sb_2Te_3$  when it is encapsulated within both bundled and discrete SWNTs with diameters ranging between 1.2 and 1.7 nm. In terms of individual filled tubes we observe a homologous series of nanocrystals that vary in an integral fashion in

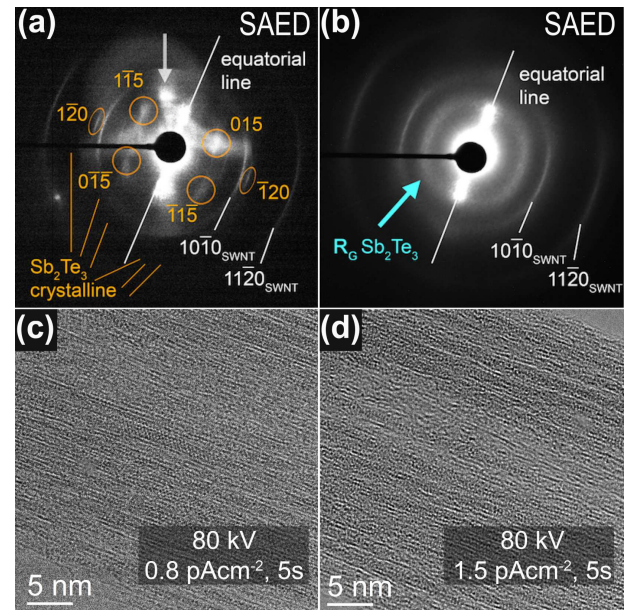


Fig. 4. (a) ED pattern ( $0.35\text{ }\mu\text{m}$  aperture) of crystalline  $Sb_2Te_3$  retained within a 25 nm diameter SWNT bundle at  $0.8\text{ pA cm}^{-2}$  electron dose. Six discrete reflections (indicated) are clearly observed for crystalline  $Sb_2Te_3$  the SWNT. Crystalline regions are clearly visible in the main image; (b) ED pattern ( $0.35\text{ }\mu\text{m}$  aperture) from the same region as (a) after electron beam irradiation at  $1.5\text{ pA cm}^{-2}$  electron dose after for a total irradiation time of 5 mins of total irradiation time. The six reflections of  $Sb_2Te_3$  are lost and replaced with a single diffuse diffraction ring (i.e.  $R_G$  corresponding to the glassy  $Sb_2Te_3$  phase). The three indicated diffraction features for the SWNTs are unchanged relative to (a) (see also Figs. 1a and c). (c) and (d) High resolution AC-TEM images of the same SWNT bundle regions as used to produce the ED patterns in (a) and (b) respectively before and after the increase in electron beam dose showing the loss of crystallinity in the latter.

terms of the number of atomic layers observed in plan view in response to SWNT diameter (i.e. Fig. 2a–d) but which share common microstructural features. Secondly, these prominent scattering features from the embedded nanocrystals apparently also contribute to the global scattering behaviour of bundles of SWNTs filled with  $Sb_2Te_3$  as they appear to have a common crystallographic origin (cf. Figs. 1c, 2f, 3c, and 4a). Thirdly, the global scattering behaviour of  $Sb_2Te_3$  encapsulated within SWNTs is significant as it allows us to monitor the *in situ* phase change characteristics of this material in response to electron beam doses ranging from  $0.8\text{ pA cm}^{-2}$  to  $1.5\text{ pA cm}^{-2}$  at an electron accelerating voltage of 80 kV. When the electron beam density is increased towards the higher value we find that the crystalline to glassy phase transformation is readily observed while the diffraction features of the encapsulating SWNTs are largely unaffected principally because the beam irradiation studies are performed below

the widely reported threshold for carbon knock-on damage of 86 keV (Fig. 4d) [14]. This latter observation is significant as, provided that the crystallinity of the encapsulated SWNTs can be demonstrated, mass-loss from the encapsulated glassy Sb<sub>2</sub>Te<sub>3</sub> phase should be minimal and reversible crystalline  $\Leftrightarrow$  glass phase transformations within SWNT should therefore be possible.

Additional characteristics of the nanotubes that are significant with regards to these experiments, concern their relative diameters and their ability to form large bundles, which is affected by their relative purity. We have selected highly pure nanotubes with a moderate diameter range from 1.2–1.7 nm for these experiments as these can template a good range of crystal fragments homologues of Sb<sub>2</sub>Te<sub>3</sub> (i.e. Fig. 2). Newly published work on SWNT encapsulated PbTe [23], has underscored this important relationship between nanotube diameter and obtained crystalline phase and orientation. Each separate microstructure formed within a particular diameter SWNT will produce a contribution to electron diffraction patterns produced from individual filled SWNTs or bundles of these. Narrow carbon nanotubes with diameters in the range 0.7–1.1 nm have very recently been shown to produce newly observed pure 1D forms of crystal growth (i.e. linear chains of CsI [24] and atomic coils of Te or Be [25, 26] in SWNTS) that may not be so readily interpretable as they cannot form crystallites 2–5 atomic layers thick but they will nonetheless improve our knowledge of phase formation on an even smaller scale than reported here. Encapsulated crystals of 2–5 atomic layers in thickness will allow us to observe crystalline to amorphous phase transitions at the smallest possible scale and this is the main conclusion from our study.

### Acknowledgments

This investigation was partially funded by the EAgLE international project (FP7-REGPOT-2013-1, Project No. 316014) and also the international project co-financed by Polish Ministry of Science and Higher Education, Grant Agreement 2819/7.PR/2013/2. J.S. and S.R.M. are grateful to additional support from EPSRC grants EP/M010643/1 and EP/J016276/1.

### References

[1] A. Sato, Y. Tsukamoto, *Nature* **363**, 431 (1993).  
 [2] H.J. Gao, K. Sohlberg, Z.Q. Xue, H.Y. Chen, S.M. Hou, L.P. Ma, X.W. Fang, S.J. Pang, S.J. Pennycook, *Phys. Rev. Lett.* **84**, 1780 (2000).  
 [3] K. Yano, T. Ikeda, *Appl. Phys. Lett.* **80**, 1067 (2002).  
 [4] Y. Cho, *Integr. Ferroelectr.* **50**, 189 (2002).  
 [5] H.J. Mamin, *Appl. Phys. Lett.* **69**, 433 (1996).  
 [6] E.B. Cooper, S.R. Manalis, H. Fang, H. Dai, K. Matsumoto, S.C. Minne, T. Hunt, C.F. Quate, *Appl. Phys. Lett.* **75**, 3566 (1999).

[7] M. Cavallini, F. Biscarini, S. Leo, F. Zerbetto, G. Bot-tari, D.A. Leigh, *Science* **299**, 531 (2003).  
 [8] C.E. Giusca, V. Stolojan, J. Sloan, F. Börrnert, H. Shiozawa, K. Sader, M.H. Rummeli, B. Büchner, S.R.P. Silva, *Nano Lett.* **13**, 4020 (2013).  
 [9] R. Carter, M. Suyetin, S. Lister, M.A. Dyson, H. Trehitt, S. Goel, Z. Liu, K. Suenaga, C. Giusca, R.J. Kashtiban, J.L. Hutchison, J.C. Dore, G.R. Bell, E. Bichoutskaia, J. Sloan, *Dalton Trans.* **43**, 7391 (2014).  
 [10] A.V. Lukashin, N.S. Falaleev, N.I. Verbitskiy, A.A. Volykhov, I.I. Verbitskiy, L.V. Yashna, A.K. Kumsov, N.A. Kiselev, A.A. Eliseev, *Nanosyst. Phys. Chem. Math.* **6**, 850 (2015).  
 [11] H.D. Yan, P. Lemmens, H. Dierke, S.C. White, F. Ludwig, M. Schilling, *J. Phys. Conf. Series* **145**, 012079 (2008).  
 [12] P. Kumar, T. Hoffman, P. Huber, P. Scheib, P. Lemmens, *J. Appl. Phys.* **103**, 024303 (2008).  
 [13] K.M. Liew, C.H. Wong, X.Q. He, M.J. Tan, *Phys. Rev. B* **71**, 075424 (2005).  
 [14] A. Zobelli, A. Gloter, C.P. Ewels, G. Seifert, C. Colliex, *Phys. Rev. B* **75**, 245402 (2007).  
 [15] M. Zhu, M. Xia, Z. Song, Y. Cheng, L. Wu, F. Rao, S. Song, M. Wang, Y. Lu, S. Feng, *Nanoscale* **7**, 9935 (2015).  
 [16] M. Winkler, X. Liu, J.D. König, S. Buller, U. Schürmann, L. Kienle, W. Bensch, H. Böttner, *J. Mater. Chem.* **22**, 11323 (2012).  
 [17] A.N. Mansour, W. Wong-Ng, Q. Huang, W. Tang, A. Thompson, J. Sharp, *J. Appl. Phys.* **116**, 083513 (2014).  
 [18] J. Sloan, D.M. Wright, H.G. Woo, S. Bailey, G. Brown, A.P.E. York, K.S. Coleman, J.L. Hutchison, M.L.H. Green, *Chem. Commun.*, 699 (1999).  
 [19] J.-F. Colomer, L. Henrad, Ph. Lambin, G. Van Tendeloo, *Phys. Rev. B* **64**, 125425 (2001).  
 [20] C. Bosch-Navarro, L.M. Perkins, R.J. Kashtiban, J.P. Rourke, I.J. Shannon, J. Sloan, *ACS Nano* **10**, 796 (2016).  
 [21] J. Sloan, A.I. Kirkland, J.L. Hutchison, M.L.H. Green, *Chem. Commun.*, 1319 (2002).  
 [22] K. N'Dri, V. Coulibaly, D. Houphouët-Boigny, J.C. Jumas, *J. Ovon. Res.* **9**, 113 (2013).  
 [23] A.A. Eliseev, N.S. Falaleev, N.I. Verbitskiy, A.A. Volykhov, L.V. Yashina, A. Kumskov, V.G. Zhigalina, A.L. Vasiliev, A.V. Lukashin, J. Sloan, N.A. Kiselev, *Nano Lett.* **17**, 805 (2017).  
 [24] R. Senga, H.-P. Komsa, Z. Liu, K. Hirose-Takai, A.V. Krashennnikov, K. Suenaga, *Nat. Mater.* **13**, 1050 (2014).  
 [25] A. Vasylenko, J. Wynn, P. Medeiros, A.J. Morris, J. Sloan, D. Quigley, *Phys. Rev. B* **95**, 121408R (2017).  
 [26] P.V.C. Medeiros, S.R. Marks, J.M. Wynn, A. Vasylenko, Q. Ramasse, D. Quigley, J. Sloan, A.J. Morris, *ACS Nano*, (2017).